Marine and Petroleum Geology 104 (2019) 361–374

Contents lists available at ScienceDirect

Marine and Petroleum Geology

journal homepage: www.elsevier.com/locate/marpetgeo

Research paper

Active degassing across the Maltese Islands (Mediterranean Sea) and implications for its neotectonics

Aaron Micallef[a,*], Daniele Spatola[a], Antonio Caracausi[b], Francesco Italiano[b], Giovanni Barreca[c], Sebastiano D'Amico[d], Lorenzo Petronio[e], Franco Coren[e], Lorenzo Facchin[e], Rita Blanos[e], Alessandro Pavan[e], Paolo Paganini[e], Marco Taviani[f,g,h]

[a] Marine Geology and Seafloor Surveying Group, Department of Geosciences, University of Malta, Msida, Malta
[b] Istituto Nazionale di Geofisica e Vulcanologia, Sezione di Palermo, Palermo, Italy
[c] Dipartimento di Scienze Biologiche, Geologiche e Ambientali, Università di Catania, Catania, Italy
[d] Seismic Monitoring and Research Group, Department of Geosciences, University of Malta, Msida, Malta
[e] Istituto Nazionale di Oceanografia e di Geofisica Sperimentale (OGS), Trieste, Italy
[f] CNR-ISMAR, Bologna, Italy
[g] Stazione Zoologica Anton Dohrn, Napoli, Italy
[h] Biology Department, Woods Hole Oceanographic Institution, Woods Hole, MA, 02543, USA

ARTICLE INFO

Keywords:
Gas seepage
Faults
Neotectonics
Maltese Islands
Mediterranean sea

ABSTRACT

The Maltese Islands, located in the central Mediterranean Sea, are intersected by two normal fault systems associated with continental rifting to the south. Due to a lack of evidence for offshore displacement and insignificant historical seismicity, the systems are thought to be inactive and the rift-related deformation is believed to have ceased. In this study we integrate aerial, marine and onshore geological, geophysical and geochemical data from the Maltese Islands to demonstrate that the majority of faults offshore the archipelago underwent extensional to transtensional deformation during the last 20 ka. We also document an active fluid flow system responsible for degassing of CH_4 and CO_2. The gases migrate through carbonate bedrock and overlying sedimentary layers via focused pathways, such as faults and pipe structures, and possibly via diffuse pathways, such as fractures. Where the gases seep offshore, they form pockmarks and rise through the water column into the atmosphere. Gas migration and seepage implies that the onshore and offshore faults systems are permeable and that they were active recently and simultaneously. The latter can be explained by a transtensional system involving two right-stepping, right-lateral NW-SE trending faults, either binding a pull-apart basin between the islands of Malta and Gozo or associated with minor connecting antitethic structures. Such a configuration may be responsible for the generation or reactivation of faults onshore and offshore the Maltese Islands, and fits into the modern divergent strain-stress regime inferred from geodetic data.

1. Introduction

Faults can act as both avenues for, and barriers to, fluid migration (Bense and Person, 2006; Hooper, 1991). Faults have been shown to provide good migration pathways for fluids in a variety of settings (Aydin, 2000; Gay and Berndt, 2007; Jolley et al., 2007; Panieri et al., 2017; Savini et al., 2009; Vogt et al., 1994; Wilson et al., 2014). The permeability structure of fault zones is a function of the original lithology being faulted, shear strain, dilation, and fracture development, and varies as a function of burial depth, fault throw, and secondary mineralisation (Fisher and Knipe, 1998; Mailloux et al., 1999; Rawling et al., 2001; Saffer, 2015; Yehya et al., 2018). Evidence for faults forming preferential pathways for vertical fluid flow include mineralisation patterns (Garven et al., 1999; Zhao et al., 2016), geothermal anomalies (McKenna and Blackwell, 2004), and expulsion of overpressured fluids (Cox, 2016; Roberts et al., 1996). In contrast, faults are also known to act as barriers to horizontal fluid flow compartmentalisation, such as in offshore hydrocarbon reservoirs (Ho et al., 2018; Knott et al., 1996) and in silicilastic sedimentary aquifers (Bense and Person, 2006; Saribudak and Hawkins, 2019). Fluid flow is a function of fault activity. Recent fault displacement leads to scarcely-cemented fault breccias and an increase in fault-zone permeability (Burnard et al., 2012; Dogan et al., 2007; Kennedy et al., 1997; Yeyya et al., 2018). Associations between fluid expulsion sites and active fault systems have

* Corresponding author. 37, Triq ta' Xmiexi, Msida, Malta.
E-mail address: aaron.micallef@um.edu.mt (A. Micallef).

https://doi.org/10.1016/j.marpetgeo.2019.03.033
Received 8 January 2019; Received in revised form 25 March 2019; Accepted 26 March 2019
Available online 04 April 2019

been shown in a wide range of settings (Géli et al., 2008; Hooper, 1991; Moore et al., 1990; Le Pichon et al., 2001; Spatola et al., 2018).

Active fluid seeps have generally been detected and characterised via direct observation and sampling. Offshore, echo-sounders have been used to record acoustic anomalies due to gas bubbles in the water column (Gentz et al., 2014; Jerram et al., 2015; Schneider von Deimling et al., 2007). Near-bottom visual observations by divers or platforms equipped with a camera, such as towed frames or Remotely Operated Vehicles, have enabled identification of active gas bubble seepage (Gasperini et al., 2012). Probes and sensors, mounted on these platforms and using gas-extraction step, biosensing or solid-state optical measurements, have been used to detect and measure dissolved methane in situ over long periods of time (Boulart et al., 2010; Gasperini et al., 2012). Discrete water samples collected with Niskin bottles have been analysed for gas chromatography, molecular composition and stable isotopes to determine the concentration and genesis of the fluids (Etiope et al., 2014; Gentz et al., 2014; Savini et al., 2009). Geochemical analyses of the sub-stratum and its interstitial waters have yielded information on rate and timing of fluid seepage (Abrams et al., 2001; Toki et al., 2004; Panieri, 2006). Satellite remote sensing imagery has been used to detect floating oil over active seeps (Espedal and Wahl, 1999) and provide estimates of seepage rates (MacDonald et al., 1993). Onshore, detection of active gas seeps and inference of their source have been based on direct soil gas measurements (Cicerone and Shetter, 1981; Maljanen et al., 2004), and on the chemical and isotopic analyses of the dissolved gas phase in groundwater bodies and springs (Italiano et al., 2009).

The Maltese Islands, located in the central Mediterranean Sea, are intersected by two systems of faults. The ages assigned to these fault systems span from the Early Miocene to mid-Pliocene and are mainly based on interpretation of poor quality offshore seismic reflection profiles (Dart et al., 1993; Illies, 1981). Due to the lack of seafloor evidence of fault displacement and insignificant historical seismicity, the fault systems are thought to be inactive and rift-related deformation is believed to have largely ceased (Dart et al., 1993; Illies, 1981). There are no reports of neotectonic movements along onshore faults (Bonson et al., 2007), and the most recent fault activity has been related to displacement of late Pleistocene-Holocene age alluvial fanglomerates along one fault in the south of Malta (Government of Malta, 1993). In our study, we integrate aerial, marine and onshore geological, geophysical and geochemical data from the Maltese Islands to: (i) document an active fluid flow system responsible for degassing of CH_4 and CO_2, (ii) demonstrate that the two fault systems were recently active, and (iii) suggest that onshore and offshore faults were either formed or reactivated by an active transtensional system.

2. Regional setting

2.1. The Pelagian Platform

The Pelagian Platform, located in the central Mediterranean Sea (Fig. 1), forms part of the African continental plate and consists of a 25–30 km thick continental crust. It extends from southern Sicily to Tunisia in the west, northern Libya in the south and the Malta Escarpment to the east (Finetti, 1982). The upper sedimentary units on the Pelagian Platform comprise Plio-Pleistocene units of terrigenous, pelagic and hemipelagic sediments that are up to 300 m thick (Max et al., 1993; Osler and Algan, 1999). Underlying these units are > 4 km thick sedimentary sequences of Miocene to Cretaceous shelf edge carbonate build ups, and Cretaceous to Triassic shallow platform carbonates (Jongsma et al., 1985; Scandone, 1981; Torelli et al., 1998). The carbonate sequences are punctuated by extensive depositional hiatuses, as well as tuffs and pillow lavas deposited during a number of volcanic episodes (Bosellini, 2002; Scandone, 1981).

The Pelagian Platform is a foreland domain that, between the Mesozoic and Cenozoic, underwent N–S compression due to the convergence of the African and Eurasian plates (Ben-Avraham and Grasso, 1991; Burollet et al., 1978; Carminati et al., 2004; Goes et al., 2004; Gueguen et al., 1998). Shortening waned during the Miocene, when deformation became mainly extensional. During the Late Miocene, three NW-SE trending grabens (Pantelleria, Malta and Linosa) started forming in the central part of the Pelagian Platform, leading to the development of the 600 km long Sicily Channel Rift Zone (Civile et al., 2008, 2010; Dart et al., 1993; Finetti, 1984; Finetti et al., 2005; Jongsma et al., 1985) (Fig. 1). The grabens have a water depth of up to 1700 m; they are filled by up to 2000 m thick Lower Pliocene-Pleistocene turbidites and are bound by sub-vertical normal and oblique faults (Civile et al., 2010). Rifting has resulted in a thinned continental crust and has been accompanied by widespread subaerial and submarine volcanic activity (e.g. Pantelleria, Linosa, Graham and Nameless banks) (Argnani, 1990; Civile et al., 2008). Three explanations have been put forward for the origin of the Sicily Channel Rift Zone: (i) The grabens are pull-apart basins developed along a major dextral wrench zone (Finetti et al., 2005; Jongsma et al., 1985; Reuther and Eisbacher, 1985); (ii) The rifting is associated with mantle convections developed during the roll-back of the African lithospheric slab beneath the Tyrrhenian Basin (Argnani, 1990; Reuther et al., 1993); (iii) Intraplate rifting related to the north-eastern displacement of Sicily away from the African continent (Illies, 1981; Winnock, 1981).

2.2. The Maltese Islands

The Maltese Islands are located in the central eastern part of the Pelagian Platform, along the northern rim of the Malta Graben (Fig. 1a). The archipelago consists of the islands of Malta, Gozo and Comino, which comprise a shallow water, Oligo-Miocene sedimentary succession of five main formations (Pedley et al., 1976). This sequence is disrupted by two normal fault systems, which have a predominant control on the subaerial geomorphology of the archipelago (Alexander, 1988) and which are closely related to the development of the Malta Graben (Illies, 1981; Reuther and Eisbacher, 1985). The most widespread system consists of ENE-WSW trending faults dipping at 55–75°. Faults belonging to this system mainly occur between Malta and Gozo, where they form a ~15 km wide horst and graben structure. The most prominent fault of this system is the Great/Victoria Fault (Fig. 1b). The second system consists of NW-SE trending, oblique flank-rift faults. The most impressive of these faults is the Maghlaq Fault, which runs along the southern coastline of Malta (Bonson et al., 2007) (Fig. 1b). The offshore faults tend to be oriented parallel to these two fault systems (Fig. 1a). Fig. 1c shows the locations and focal mechanisms of earthquakes that occurred on, and in the vicinity of, the Maltese Islands between 2010 and 2018. Only nine focal mechanisms could be determined, and these are dextral strike-slip with an extensional component. Two of these coincide with the Maghlaq Fault and a NW-SE trending escarpment located north of Malta.

3. Materials and methods

3.1. Aerial data

In November 2017, an aerial survey was carried out to determine CH_4 and CO_2 concentrations in the atmosphere across the Gozo Channel (Fig. 2a). Data were acquired with a Los Gatos Research Ultraportable Greenhouse Gas Analyser carried on-board of a Cessna 172 aircraft. This instrument provides accurate CH_4 and CO_2 measurements at levels up to 10% mole fraction (without dilution) and without reducing precision and sensitivity at typical ambient level. The error margin of the instrument is < 2 ppb for CH_4 and < 300 ppb for CO_2. The instrument inlet pipe was placed on the wing leading edge near a fresh air inlet used for the conditioning of the cockpit. This allowed us to sample undisturbed and uncontaminated air. The flight path entailed 22 parallel lines over an area of 30 km^2 between Malta and Gozo. The height of the flight was set to 500 feet and the speed of the aircraft was

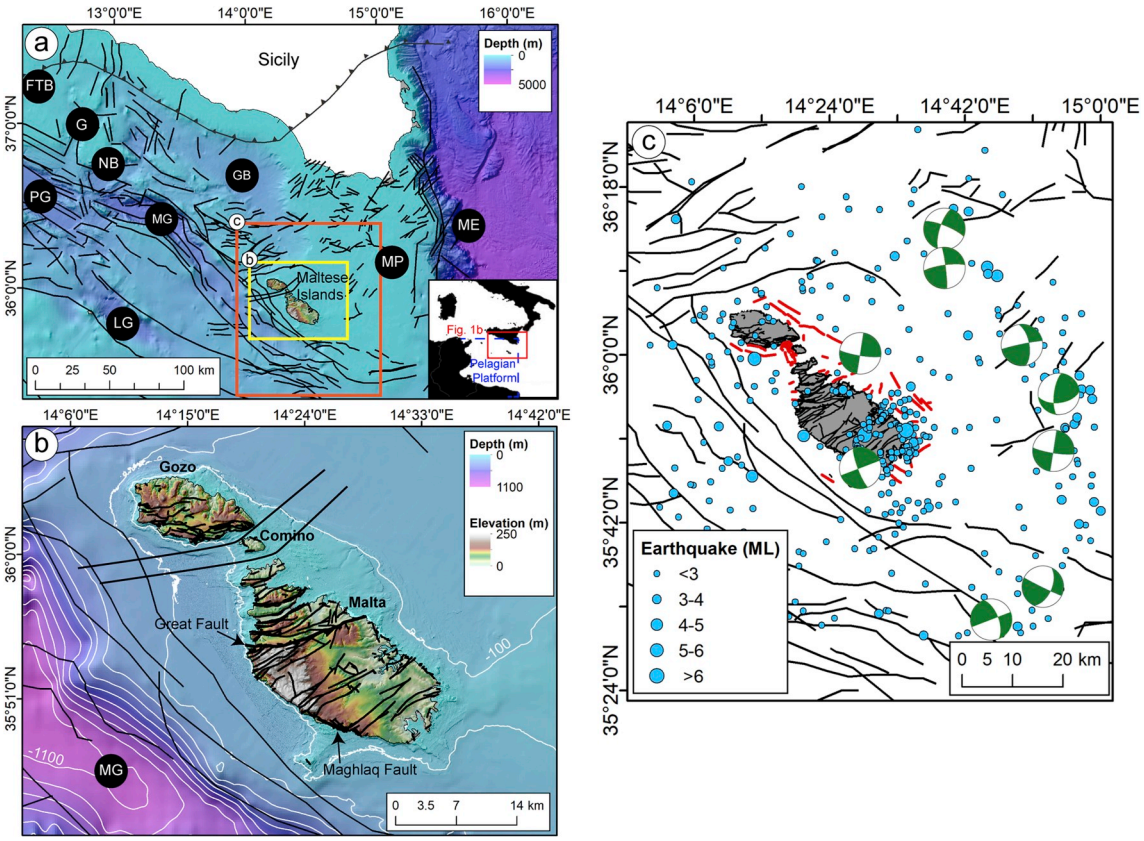

Fig. 1. Study area and regional setting. (a) Bathymetric map of the northern section of the Pelagian Platform (central Mediterranean Sea), showing the principal morphological and structural features (faults are denoted in black). Sources: Illies (1981); Gardiner et al. (1995); Lipparini et al. (2009); Civile et al. (2010). Background bathymetry from EMODnet bathymetry (http://www.emodnet-bathymetry.eu). FTB: Fold and Thrust Belt, G: Graham Bank, PG: Pantelleria Graben, NB: Nameless Bank, MG: Malta Graben, LG: Linosa Graben, GB: Gela Basin, MP: Malta Plateau, ME: Malta Escarpment. (b) Topographic map of the Maltese Islands and bathymetric map of the surrounding seafloor (isobaths in white at 100 m intervals). Faults are denoted in black (Source: Government of Malta, 1993). (c) Location, magnitude (in light blue) and focal mechanisms (in green) of earthquakes recorded between 2010 and 2018. Earthquakes moment tensor solutions were calculated by waveform inversion (Zhu and Helmberger, 1996) using the permanent Malta Seismic Network and INGV stations located in Sicily. Earthquake location is obtained by automatically analysing the 3-component single-station polarization data within 10–15 km from WDD station may be affected by large location error since back-azimuth estimations are not always accurate (Agius and Galea, 2011). Faults are denoted in black. Escarpments identified in this study (4.1.2) are shown in red. (For interpretation of the references to colour in this figure legend, the reader is referred to the Web version of this article.)

maintained at 70 knots. The flight was performed in good weather conditions, with clear sky and low wind velocities.

We also acquired one air sample at sea level in the Gozo Channel (Fig. 2b) using a two-valve glass bottle. The chemical composition and concentration of the gases was measured using the method explained in section 3.2.5.

3.2. Marine data

Our marine data were acquired during seven research cruises: HMS Roebuck (2006), MEDCOR (2009), RICS10 (2010), DECORS (2011), Gozo Channel (2016) & (2017) and MARCAN Malta (2018) on board the research vessels HMS Roebuck, R/V Urania, R/V Hercules, M/V Midas and M/V Goldfinder (Fig. 2).

3.2.1. Bathymetric data

An overall area of ~330 km^2 of seafloor was surveyed using hull-mounted multibeam echo-sounder systems (Fig. 2a). The instruments used to acquire each multibeam echo-sounder data set and the cell size of the processed grids are listed below:

- HMS Roebuck (2006), Kongsberg-Simrad EM-1002, grid size of 10 m;
- MEDCOR (2009), Kongsberg-Simrad EM-710, grid size of 5 m;
- RICS10 (2010), Kongsberg-Simrad EM-3002D, grid size of 1 m;
- DECORS (2011), Kongsberg-Simrad EM-710, grid size of 1 m;
- Gozo Channel (2016), Reson SeaBat 7125, grid size of 2 m.

Bathymetry was derived from the MBES surveys by accounting for sound velocity variations and tides, and by implementing basic quality control. Bathymetric data were exported as 32-bit rasters. Our data sets were complemented by ~430 km^2 of bathymetric data acquired with a Hawkeye IIb bathymetric LiDAR sensor and an interferometric swath system (Kongsberg GeoSwath), collected as part of the project "Development of Environmental Monitoring Strategy and Environmental Monitoring Baseline Surveys" funded by ERDF-156. The cell size for these data sets is 10 m.

3.2.2. Acoustic profiles

980 km of acoustic profiles were collected using three systems (Fig. 2a): (i) a pole-mounted Innomar SES-2000 compact sub-bottom profiler, with primary and secondary frequencies of 100 kHz and 8 kHz, respectively; (ii) hull-mounted 16 transducer CHIRP-II profiler (BENTHOS DATASONICS Mod. CAP-6600) with an operating frequency of 3.5 kHz; (iii) a Boomer seismic source with an operating frequency of 3.5 kHz and a 50 m long Geo-Sense mono-channel streamer with a sensitivity of ± 2 dB (Fig. 2b). The Boomer data were processed with a conventional mono-channel processing sequence that included band pass filtering, gain recovery, seismic signal enhancement, attenuation of noise eddy currents, and seawater column mute.

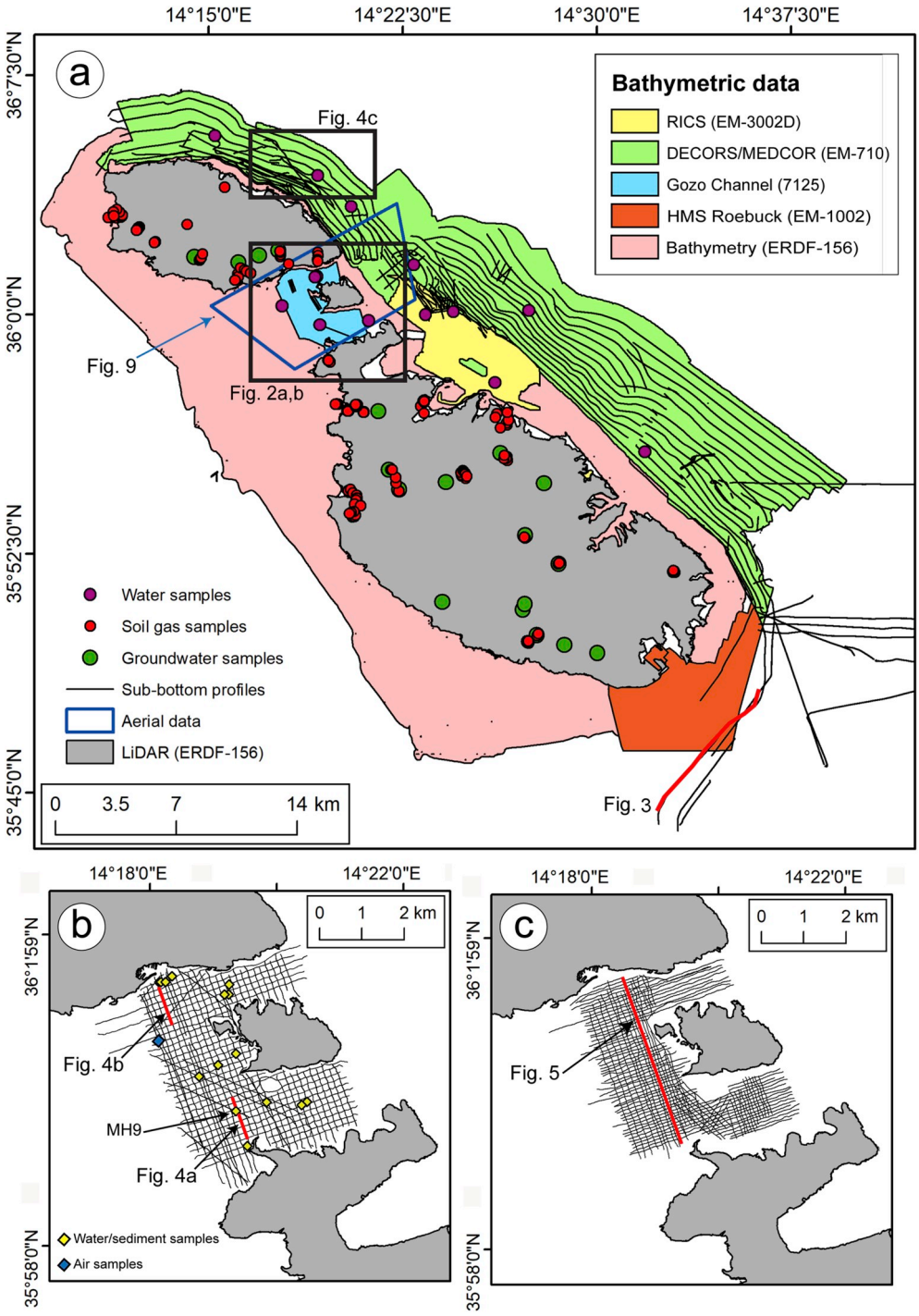

Fig. 2. (a) Spatial coverage of the aerial data, marine data (multibeam echo-sounder data, sub-bottom profiles, water samples) and onshore data (groundwater and soil gas samples; LiDAR data). (b) Spatial coverage of the Boomer acoustic profiles, water and sediment samples, and air sample. c) Spatial coverage of the multichannel seismic reflection profiles.

3.2.3. Multi-channel seismic reflection profiles

240 km of profiles have been acquired from the Gozo Channel using a mini GI gun with a total volume of 60 cu. in. (1 l) (Fig. 2c). A shot point distance of 15.625–18.750 m and a recording length of 2 s were used. Data were recorded using a 300 m long digital streamer with 96 channels, with a channel distance of 3.125 m. The fold coverage ranged between 8 and 9.6 traces per CDP. The processing sequence included amplitude recovery, bandpass filtering, CDP sorting, pre-stack deconvolution, velocity analyses, normal move out correction, and stacking.

3.2.4. Seafloor sediment samples

Seventeen superficial sediment samples were collected using a 5 l modified Van-Veen Grab (Fig. 2b). These samples were described, photographed and sub-sampled on-board. Grain size distribution of the samples was analysed using sieves, following the ASTM D0422, and a Malvern Mastersizer 3000. Five sediment samples (Site 1, Site 2, Site 8, Site 9, and MH9) were analysed using X-ray diffraction (XRD) to determine the qualitative and semi-quantitative mineralogical composition of the carbonate fraction. Mineral identification was performed on dried and ground sub-samples using a Rigaku MiniFlex XRD

diffractometer.

3.2.5. Water column samples

Twenty four water column samples were collected with a 5 l Niskin bottle (Fig. 2a–b). Immediately after the Niskin bottle returned on deck, a drawtube was pre-rinsed with sample water and attached to the Niskin bottle's spigot. Glass and PET flasks were then filled and overflowed, avoiding the formation of air bubbles in order to prevent air contaminations. In the PET flasks, a headspace was created and one drop of saturated HCl was added to the sample. All the flasks were stored in the dark. Geochemical analysis were performed in the laboratories of the Istituto Nazionale di Geofisica e Volcanologia (sezione di Palermo). The chemical composition and concentration of the gases dissolved in seawater samples were determined by using the method in Capasso and Inguaggiato (1998). For the gas chromatography analyses, the sample was split in two aliquots. The first was analysed for O_2, N_2, CH_4 and CO with an Agilent 7890B with two columns in series (Poraplot U 25 m × 0.53 mm and Molsieve 5A 25 m × 0.53 mm) fluxed by Ar (detectors TDC and FID with methaniser). The second aliquot was analysed for CO_2 and H_2S by a microGC module (MicroGC 3000) equipped with Poraplot U column (15 m) fluxed by He (detector TCD). Calibration was made with certified gas mixtures. Analytical precision was always better than ± 3%. The detection limit was ~0.3 ppm for CO and CH_4, 30 ppm for CO_2, and 200 ppm for O_2 and N_2. The isotopic ratio of oxygen ($\delta^{18}O$) was measured using a mass spectrometer Thermo Delta V Plus coupled to a GasBench II that exploits the principle of the head space. For the determination of hydrogen isotopic ratio (δD), we utilised a mass spectrometer Delta Plus XP coupled with a TC/EA reactor. The analytical precision is better than ± 0.1% and ± 1% for $\delta^{18}O$ and δD, respectively. Isotope ratios are expressed using delta notation as relative differences in parts per mil (δ values %) from Standard Mean Ocean Water (SMOW).

3.3. Onshore data

3.3.1. Topographic LiDAR data

Topographic LiDAR data were acquired during a 5.5 h flight in February 2012 using an IGI LiteMapper 6800 system (Fig. 2a). The data have a cell size of 1 m and were collected as part of the project "Development of Environmental Monitoring Strategy and Environmental Monitoring Baseline Surveys" funded by ERDF-156.

3.3.2. Groundwater samples

Water samples were collected at eighteen onshore sites (Fig. 2a), from either boreholes or galleries (Ta' Kandja, Malta), in January 2014. The depth of the sampled water ranges between 29 and 234 m below the surface. Samples for isotopic measurements were collected and stored in PET bottles and in triplicate: one sample as-is, one filtered through Millipore 0.45 μm filters, and one filtered and acidified with suprapure-grade HNO_3. Samples collected for the extraction of the dissolved gases were stored in 240 ml pyrex bottles sealed in the field using silicon/Teflon septa and purpose-built pliers. Details on the methodology and instrumentation are described in Italiano et al. (2013, 2014).

The water isotopic composition ($\delta^{18}O$ and δD) of unfiltered samples was determined by mass-spectrometry and expressed in ‰ with respect to the international Vienna Standard Mean Ocean Water (V-SMOW). The dissolved gases were extracted following the equilibration method (Capasso and Inguaggiato, 1998). To prevent atmospheric contamination, all samples were stored upside down with necks submerged in water until the laboratory procedures were initiated. The chemical composition of the dissolved gas phase was obtained from the gas-chromatographic analyses by taking into account the solubility coefficients of each gas species (Bunsen coefficient "β", cc gas STP/ml water (cubic centimetres at standard temperature and pressure)), the volume of gas extracted and the volume of the water sample (more details are available in Italiano et al. (2009, 2014). Measurements of water isotopic composition and dissolved gas chemistry and concentration were carried out by using the same methodology described in section 3.2.5.

3.3.3. Soil gas measurements

Seventy nine soil gas measurements were carried out across the Maltese Islands (Fig. 2a). The active method was adopted, whereby soil gas is collected by a pump at a constant flow rate and driven through a pipe, 2.5 cm^2 in cross-section, which is inserted at a depth of about 0.5 m in the soil. The CO_2 concentration value of the analysed gas mixture (soil CO_2 and air) was taken when it reached steady state (constant value). The concentration is related to the CO_2 flux by the relationship:

$$\Phi t = F.CD \quad (1)$$

where Φt is the CO_2 flux, CD is the measured CO_2 concentration, and F is the flow rate of the pump. Since our objective was to identify the presence of a positive CO_2 flux towards the atmosphere, only the flow rate of the pump and the CO_2 concentration were taken into consideration. A ± 10% uncertainty was estimated by repeated measurements at the same site.

4. Results

4.1. Marine data

4.1.1. Sub-seafloor seismic facies and anomalies

The acoustic profiles exhibit two man facies (Fig. 3, 4a-b). The shallower one, facies A, reaches a maximum thickness of 0.05 s (TWTT) and consists of sub-parallel, high amplitude reflectors with good lateral continuity. We correlate this facies with post-Last Glacial Maximum medium to fine sands (Micallef et al., 2013). The deeper facies, facies B,

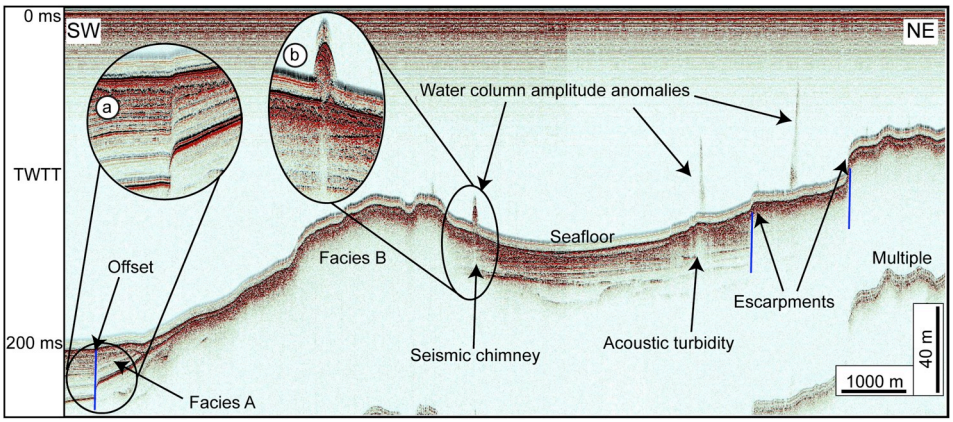

Fig. 3. Acoustic profile showing water column amplitude anomalies, seismic chimney, acoustic turbidity and offset seismic reflectors (denoted by blue lines). The facies on either side of the offset in (a) have different thicknesses. Location of the acoustic profile is shown in Fig. 2a. (For interpretation of the references to colour in this figure legend, the reader is referred to the Web version of this article.)

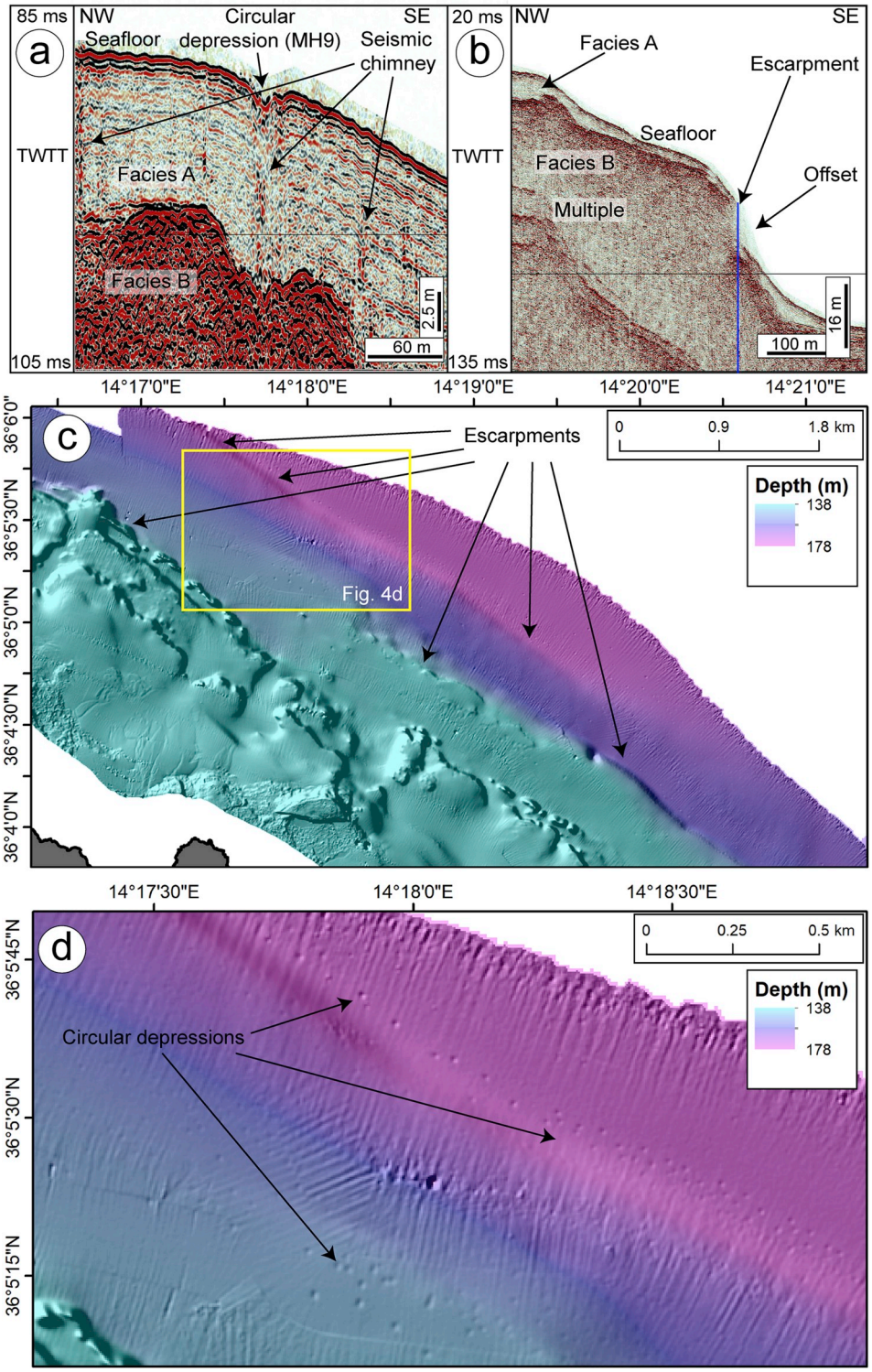

Fig. 4. Seafloor and sub-seafloor anomalies and structures. (a) Acoustic profile (Boomer) showing a circular depression and seismic chimneys underneath. Location of the acoustic profiles is shown in Fig. 2b. (b) Acoustic profile (Boomer) showing an escarpment and an offset seismic reflector (denoted by blue line). Location of the acoustic profiles is shown in Fig. 2b. (c) Bathymetric map of seafloor offshore NE Gozo showing NW-SE trending escarpments. (d) Zoom of the bathymetric map in (c) showing circular depressions, most of which are aligned NW-SE. (For interpretation of the references to colour in this figure legend, the reader is referred to the Web version of this article.)

shows very high amplitudes along the top with seemingly insufficient signal penetration beneath; it correlates with Late Miocene carbonates. Correlations are based on information from boreholes drilled offshore Comino (Infrastructure Malta, personal communication, October 2018). These two facies can also be identified in the multi-channel seismic reflection profiles (Fig. 5). Reflectors in these two facies, as well as those underlying them, are offset vertically in the Gozo Channel or to the east and south of Malta (Figs. 3, 4b and 5). By correlating offsets that showed the same dip and displacement across parallel seismic reflection profiles, we were able to map the main trend of the offsets as 38 lineaments. Sub-seafloor offsets coincide with escarpments on the seafloor (see section 4.1.2). The offsets reach the maximum penetration of the seismic signal (~1 s TWTT).

Facies A and B are also affected by two types of acoustic anomalies that disturb the lateral continuity of the seismic reflectors. The first type are seismic chimneys (up to 15 m wide) (Figs. 3 and 4a), whereas the second type comprise acoustic turbidity that extends laterally up to 2 km (Fig. 5). Both anomalies reach the maximum penetration of the seismic signal (~1 s TWTT). Acoustic turbidity can be correlated across parallel seismic reflection profiles.

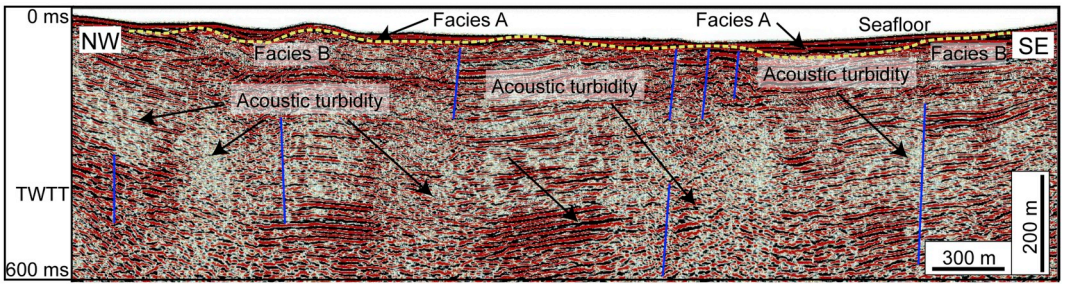

Fig. 5. Multichannel seismic reflection profile showing extensive acoustic turbidity zones and offsets (denoted by blue lines) in the Gozo Channel. Facies A and B, interpreted from the acoustic profiles, are shown. The reflector separating the two facies is denoted by a yellow dashed line. Location shown in Fig. 2c. (For interpretation of the references to colour in this figure legend, the reader is referred to the Web version of this article.)

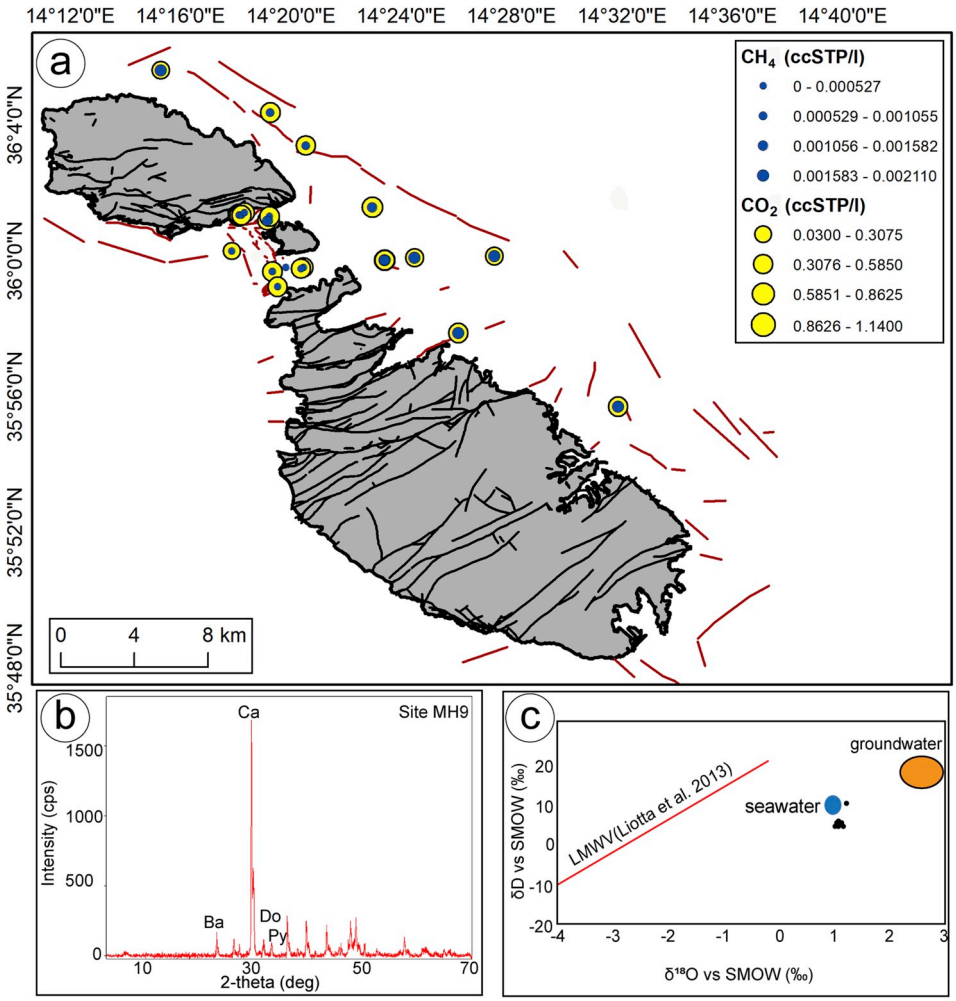

Fig. 6. Water column and sediment chemistry. (a) Measured concentrations of CH_4 and CO_2 in the water column samples. Red lines represent escarpments identified from multibeam echo-sounder data. (b) Diffractogram of sample MH9 (intensity in count per second vs 2-theta in degrees). c) δD vs $\delta^{18}O$ plot for water column samples. Data points from our study are denoted by black dots. Plotted data for groundwater, seawater and Local Mediterranean Water Values (LMWV) are from Liotta et al. (2013). (For interpretation of the references to colour in this figure legend, the reader is referred to the Web version of this article.)

4.1.2. Seafloor morphology

The seafloor predominantly consists of flat to gently sloping terrain that comprises 85 rectilinear escarpments oriented NW-SE, W-E or SW-NE (Figs. 3, 4b-c). The escarpments to the east and west of Malta are predominantly oriented NW-SE; they are up to 13 km long and 50 m high with slope gradients of > 60°. To the north and south of the Maltese Islands, the escarpments are up to 10 km long, 100 m high, up to 80° in slope gradient, and predominantly oriented SW-NE. The Gozo Channel hosts 37 quasi-linear escarpments that are predominantly oriented NW-SE, up to 700 m long, 45 m high, and 80° in slope gradient.

The seafloor also hosts 1026 circular to ellipsoidal depressions (Fig. 4c–d). Of these, 63% are located to the north-east of the Maltese Islands and 21% to the north of Gozo; the remaining 3% and 13% are located to the south-east of Malta and in the Gozo Channel, respectively. The highest depression densities (up to 35 per km^2) are observed offshore NE Gozo and in the Gozo Channel. The depressions occur at depths of 20–205 m, and they are up to 100 m wide and 3 m deep. The depressions generally cluster in NW-SE or WSW-ENE orientations, and appear to coincide with fine to medium sand cover (see Micallef et al. (2013)).

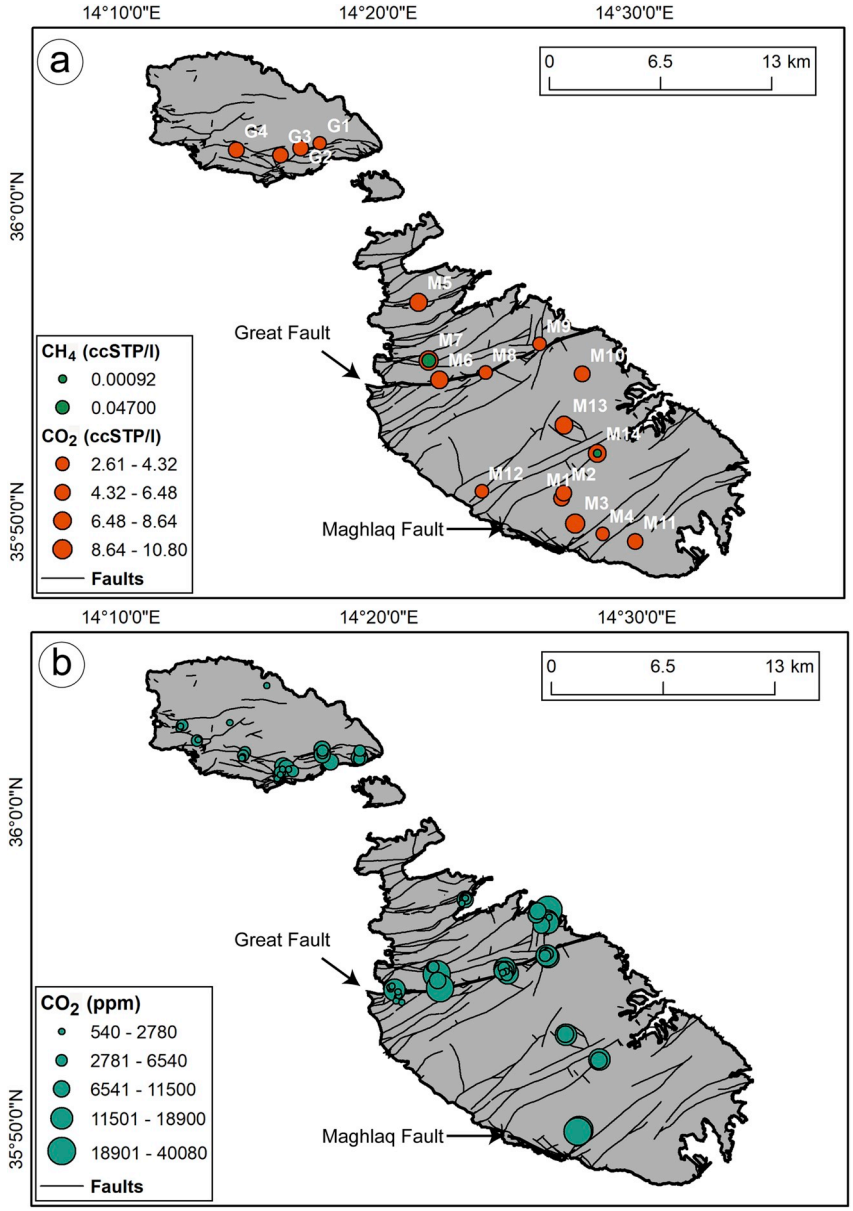

Fig. 7. Onshore water and gas chemistry. (a) Measured concentration of CH_4 and CO_2 in the onshore groundwater samples. (b) Concentration of CO_2 derived from soil gas measurements (adapted from Birhane (2016) and Gauci (2015)).

4.1.3. Seafloor sediments

Sediments collected from the seafloor depressions in the Gozo Channel predominantly consist of poorly to moderately well sorted fine to coarse sands. The samples that were analysed with XRD are mainly composed of carbonates associated with detrital minerals (clays) and minor authigenic phases (mostly barite and pyrite) (Fig. 6b). Calcite represents the dominant carbonate phases and is associated with minor quantities of dolomite (Fig. 6b).

4.1.4. Dissolved gases and water chemistry

Gas concentrations in the water samples are shown in Fig. 6a and Table 1 (Supplementary materials). Concentrations of CH_4 and CO_2 dissolved in seawater are above 4.79×10^{-5} ccSTP/l and 0.43 ccSTP/l, respectively, showing that both the volatiles are more enriched than seawater in equilibrium with the atmosphere (ASSW = Atmosphere Saturated Seawater; Capasso and Inguaggiato, 1998). The highest concentrations were recorded to the north-east of Malta (Fig. 6a). The isotopic signatures of oxygen and hydrogen for the collected seawater samples show a composition that is comparable to the Modern Mediterranean Seawater (Fig. 6c).

4.1.5. Water column amplitude anomalies

In the acoustic profiles we identified 43 water column amplitude anomalies. These anomalies consist of straight or inclined high-amplitude acoustic scattering that extend upwards from the seafloor (Fig. 3). None of the acoustic anomalies appear to reach the sea level. The majority of these anomalies were recorded in the Gozo Channel, with the rest located to the NE of Malta.

4.2. Onshore data

4.2.1. Dissolved gases and water chemistry

Atmospheric gases (O_2 and N_2) dominate the composition of the gas phase dissolved in shallow groundwater samples (Table 2 – Supplementary materials). A substantial amount of volatiles of different origin than the atmosphere, derived from gas/water interaction processes within the water bodies, is recognised as a common feature of almost all the sampled waters. After the atmospheric gases, the most

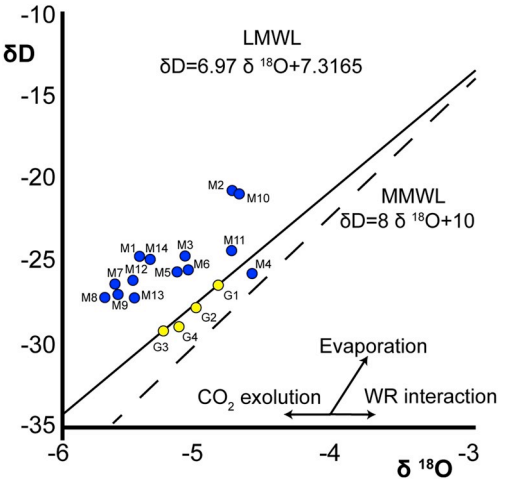

Fig. 8. δD vs. $\delta^{18}O$ plot for onshore groundwater samples. Local Mediterranean Water Line (LMWL) and Mean Mediterranean Water Line (MMWL) from Liotta et al. (2013).

abundant gas in the shallow groundwater samples is CO_2, with concentrations of 2.61–10.78 ccSTP/l (Fig. 7a). CH_4 was only detected in two samples (Fig. 7a).

The isotopic composition (Fig. 8) shows that most of the groundwater samples fall on the Local Mediterranean Water Line (LMWL).

4.2.2. Soil gas chemistry

Soil degassing measurements carried out in Malta and Gozo highlight the presence of active CO_2 emission, the concentration of which ranges between 540 and 40080 ppm for Malta, and between 660 and 8780 ppm for Gozo (Fig. 7b). The highest CO_2 concentrations were recorded along the Great and Maghlaq Faults.

4.3. Aerial data

The spatial distribution of CH_4 and CO_2 concentrations across the Gozo Channel is shown in Fig. 9. Values range between 1.850 and 1.991 ppm for CH_4, and between 403 and 406 ppm for CO_2. The dispersion of a single measurement value is in the range of $4.036–4.050 \times 10^{-2}$ ppm, and the precision of the instrument is of the order of 1.5×10^{-3} ppm. The highest concentrations of these gases occur as SW to NE elongated anomalies located between Gozo and Comino. The anomalies appear to partly correlate with the flight path. However, in view of the low line spacing used and the fact that the same point was covered more than once by different fly overs, the correlation is only geometrical, the generation of artefacts has been reduced and interpolation artefacts were minimised. Our measurements are also not correlated with the wind direction, which during the day of the survey blew from WNW at a velocity of 5–7 knots. The gridding algorithm used was a conservative one and based on a moving average. The concentrations of CH_4 and CO_2 from the ship-borne air measurement are 2.970 ppm and 1600 ppm, respectively.

4.4. Spatial correlation between observations

Onshore, sites with groundwater CO_2 and CH_4 anomalies and CO_2 degassing coincide with known faults (Fig. 7). Offshore, atmospheric CO_2 and CH_4 anomalies in the Gozo Channel are spatially associated with water column amplitude anomalies, offsets in seismic reflection profiles, escarpments, depressions, seismic chimneys, and acoustic turbidity zones (Fig. 10). CO_2 and CH_4 anomalies in the water column are spatially associated with CO_2 and CH_4 anomalies in the atmosphere and seafloor depressions. The seafloor depressions are aligned with escarpments and offsets in seismic reflection profiles, particularly to the NE of Gozo and Malta, and spatially correlate with seismic chimneys and acoustic turbidity zones (Fig. 10).

5. Discussion

5.1. Type and age of offshore faults

We interpret the offset seismic reflectors in the sub-seafloor marine data as faults, and the escarpments in the multibeam bathymetry data as their topographic expressions (Figs. 3, 4b and 5, 10). The sub-seafloor marine data suggest that the majority of these faults are extensional and belong to either the WSW-ENE or NW-SE fault systems onshore (Fig. 11). The focal mechanisms of earthquakes in the vicinity of the faults offshore north Malta and in the south of Malta indicate dextral transtensional deformation (Fig. 1c). 90% of the mapped offshore faults are likely structures that have recently been active (last 20 ka) because they displace facies A (we assume that sedimentation covered all existing topography) and are associated with seafloor escarpments. Only one-fifth of the offshore faults constitute extensions of onshore faults; 75% of these are oriented WSW-ENE, whereas the other 25% are oriented NW-SE. The fault inferred from the offset shown in Fig. 3a connects with the Maghlaq Fault and exhibits strike-slip deformation.

5.2. Nature and activity of the fluid flow system

Six types of evidence indicate that the degassing across the Maltese Islands is recent or presently active: (i) amplitude anomalies in the water column (Figs. 3 and 10), which we interpret as acoustic scattering by bubbles in the water associated with active seepage from the seafloor (e.g. Ceramicola et al., 2018; Sauter et al., 2006); (ii) the occurrence of authigenic phases (barite and pyrite) in seafloor sediment samples (Figs. 6b and 10), which suggest active, slow-flux gas systems (e.g. Bezrodnykh et al., 2013; Roberts et al., 2006); (iii) CO_2 and CH_4 anomalies in the seawater samples (Fig. 6), which are higher than air-satured seawater values (Coltelli et al., 2016; Correale et al., 2012; Gasperini et al., 2012; Savini et al., 2009); (iv) CO_2 and CH_4 anomalies in the atmosphere above the Gozo Channel (Fig. 9b–c); (v) CO_2 and CH_4 anomalies in onshore groundwater samples (Fig. 7a); CO_2 values are well above the equilibrium with ASW (0.24 ccSTP/l H_2O, and CH_4 concentrations are 2–3 magnitudes above ASW (Weiss, 1974); (vi) CO_2 degassing in soils onshore (Fig. 7b).

The seafloor depressions, which we interpret as pockmarks, provide additional evidence of escaping gases (Hovland et al., 2002; Judd and Hovland, 1992, 2007; King and MacLean, 1970). We interpret the sub-seafloor acoustic anomalies observed in the seismic reflection profiles as fluid flow pathways – the seismic chimneys as pipe structures and the wide acoustic turbidity zones as a result of the attenuation of acoustic energy by gas in the pore space, which causes chaotic reflections (Aloisi et al., 2004; Bünz et al., 2012; Goswami et al., 2017; Holland et al., 2003).

We therefore propose that the Maltese Islands host an active fluid flow system. This involves the upward migration of gases through the carbonate bedrock and overlying sedimentary layers via focused pathways, such as faults and pipe structures (e.g. Gasperini et al., 2012; Gay et al., 2012; Saffer, 2015). Diffuse pathways are also important for gas migration and are likely associated with fractures in the carbonate bedrock (e.g. Dimmen et al., 2017). Where gases are expelled in sand-covered areas offshore, they form pockmarks. They do not form in other parts of the study area, which comprise bedrock or gravel-sized maërl (Micallef et al., 2013). Where water depths are lower than a few tens of metres, the gases rise through the water column and reach the atmosphere. Fluid escape is spatially variable, with the highest fluxes (based on concentrations and density) occurring to the NE of Gozo and between south Gozo and S Malta.

The sources of the gases are difficult to determine without carrying

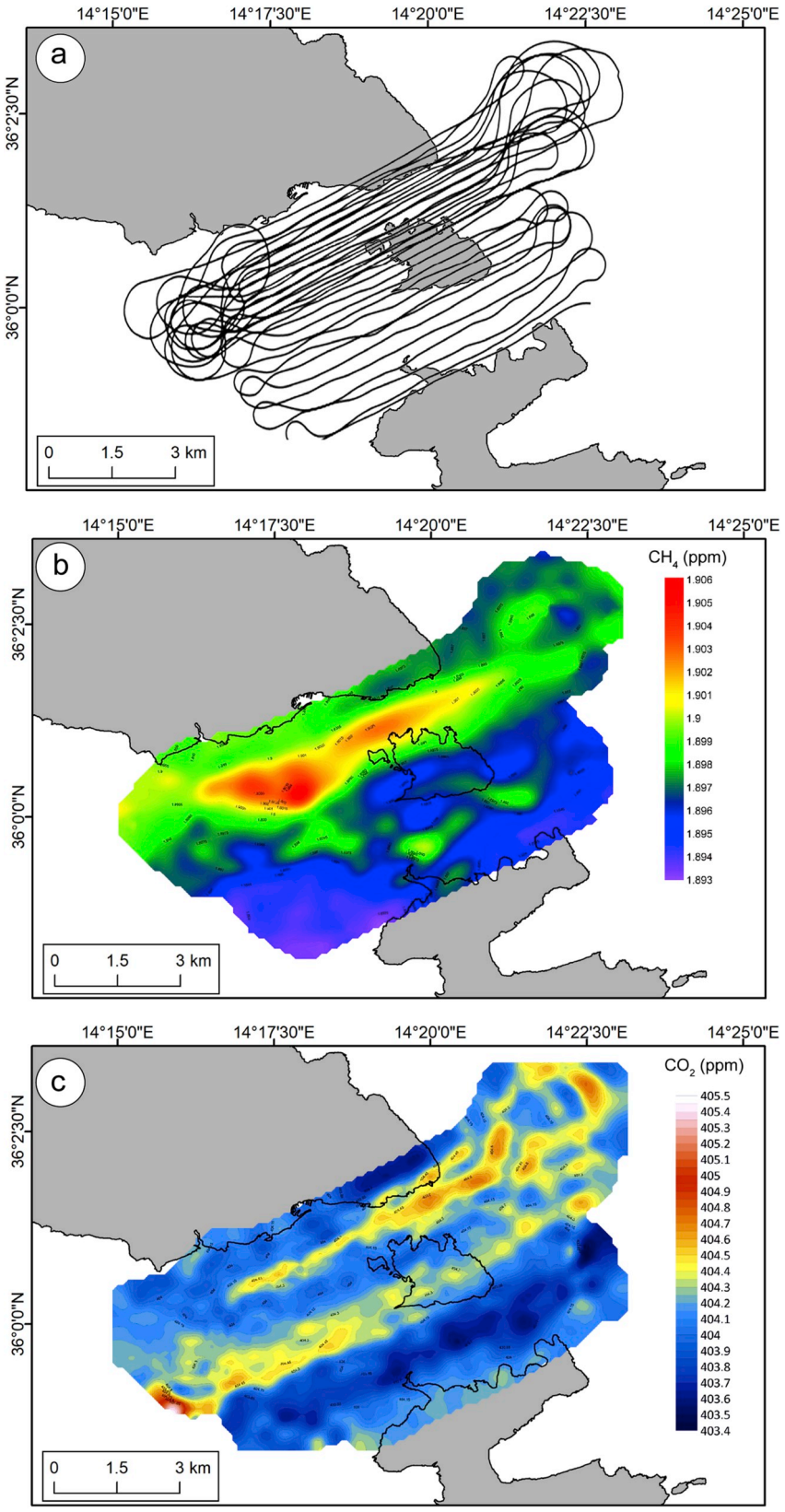

Fig. 9. (a) Flight path for aerial survey. Atmospheric concentration of (b) CH_4 and (c) CO_2 (in ppm). Values range between 1.850 and 1.991 ppm for CH_4, and between 403 and 406 ppm for CO_2. The highest concentrations of these gases occur as SW to NE elongated anomalies located between Gozo and Comino.

out more detailed geochemical analyses. CO_2 is the most abundant gas species in crustal environments. It originates from the degradation of organic matter or is degassed by active volcanic and active tectonic systems through faults and fractures (e.g., Evans and Wong, 1992; Kennedy et al., 1997; Italiano et al., 2000; Caracausi et al., 2005). CH_4 seepage is generally associated with bacterial degradation of organic

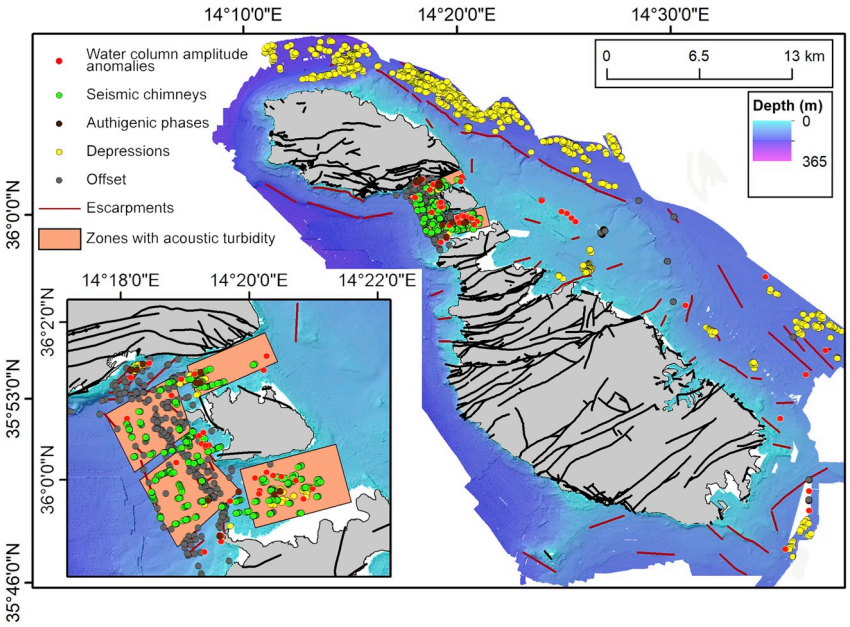

Fig. 10. Identified seafloor and sub-seafloor features across the study area shown on a shaded relief bathymetric map of the seafloor. Inset shows a zoomed section of the Gozo Channel. Onshore faults are shown in black.

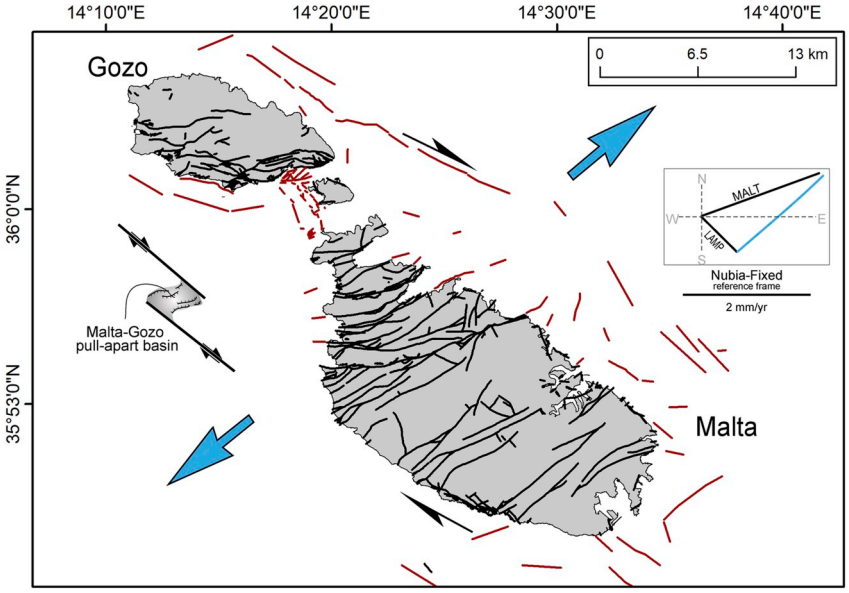

Fig. 11. Proposed transtensional fault scenario and its relation to the present strain-stress regime across the Maltese Islands (derived from available Global Navigation Satellite System velocity field (Meccariello et al., 2017)). Inset on the left shows a cartoon of a scenario with two right-stepping, right-lateral NW-SE trending faults binding a pull-apart basin. Inset on the right shows vectors decomposition (LAMP: Lampedusa, MALT: Malta), which indicate that the area is undergoing stretching in a N50E direction (blue arrows). Onshore faults are shown in black whereas offshore faults, inferred from multibeam echo-sounder and seismic reflection data, are shown in dark red. (For interpretation of the references to colour in this figure legend, the reader is referred to the Web version of this article.)

matter at low temperatures, gas hydrate destabilisation, or thermogenic fluids produced from organic precursors at high temperature and pressure (e.g., Davis, 1992; Judd and Hovland, 2007; Milkov and Etiope, 2018).

5.3. Implications for the neotectonics of the Maltese Islands

The occurrence of active gas seepage leads us to propose that the faults intersecting, or in the vicinity of, the Maltese Islands are permeable and thus recently displaced. To explain our observations of gas seeping from both ENE-WSW and NW-SE trending structures, we need a scenario where both fault systems on the Maltese Islands are simultaneously active. One such scenario entails a transtensional fault system (Fig. 11). This could comprises two right-stepping, right-lateral NW-SE trending faults (fault offshore the eastern coasts of Gozo, Comino and Malta; the Maghlaq fault and its offshore extension), binding a pull-apart basin between the islands of Malta and Gozo (Fig. 11). Alternatively, it could comprise two parallel right-lateral strike-slip faults and associated minor connecting antitethic (left-lateral) structures. Our proposed scenario is supported by the dextral strike-slip focal mechanisms of recent earthquakes in the vicinity of faults offshore north Gozo (Fig. 1c), as well as by geodetic data (Fig. 11 - inset). Horizontal velocity fields obtained by Global Navigation Satellite System and Global Positioning System stations reveal that the strain-rate field across the eastern Sicily Channel is extensional and that stretching is taking place between Lampedusa and the Maltese Islands at a rate of 1.4 mm per year in a SW-NE direction (Meccariello et al., 2017; Palano et al., 2012). This implies an active, diverging strain-stress regime across the Maltese Islands, albeit with a low deformation rate. It is likely that faults onshore and offshore the Maltese Islands were formed, or are being reactivated, by this modern stress field. The proposed transtensional fault system likely forms part of a more extensive fault system to the south (Illies, 1981; Jongsma et al., 1985; Dart et al., 1993) and represents one of the best configurations for fluid ascent and

venting (Evans and Wong, 1992; Kennedy et al., 1997; Maloney et al., 2015).

6. Conclusions

We have integrated aerial, marine and onshore geological, geophysical and geochemical data to document an active fluid flow system onshore and offshore the Maltese Islands. The system entails the upward migration of CH_4 and CO_2 through carbonate bedrock and overlying sedimentary layers via focused pathways, such as faults and pipe structures, and possibly via diffuse pathways such as fractures. Where the gases seep offshore, they form pockmarks in sand-covered seafloor. Where water depths are lower than a few tens of metres, the gases reach the atmosphere.

We also mapped 85 faults offshore the Maltese Islands that belong to either the WSW-ENE or NW-SE fault systems onshore. Geophysical data indicate that the majority of these faults were active during the last 20 ka and underwent extensional to transtensional deformation. The migration of gases implies that the onshore and offshore faults are permeable, and that the two fault systems were active recently and simultaneously. The best structural configuration that can explain the latter is a transtensional system involving two right-stepping, right-lateral NW-SE trending faults, either binding a pull-apart basin between the islands of Malta and Gozo or associated with minor connecting antitethic structures. Such a configuration, which may be responsible for the formation or reactivation of faults onshore and offshore the Maltese Islands, fits into the modern divergent strain-stress regime derived from Global Navigation Satellite System and Global Positioning System station data.

Data statement

The data used are listed in the tables and figures. The acoustic profiles are available from the corresponding author upon reasonable request. Access to the Boomer acoustic profiles and multichannel seismic reflection data from the Gozo Channel is restricted for privacy purposes; readers can apply to sarah.a.pace@infrastructuremalta.com for access.

Acknowledgments

We are grateful to the Hydrographic Office of the Malta Maritime Authority, Infrastructure Malta and Planning Authority for providing access to their data. The study also contains public sector information, licensed under the Open Government Licence v. 2.0, from the United Kingdom Hydrographic Office. The data presented should not be used for navigation. We kindly acknowledge captain, crew and scientific party of R/V Urania, R/V Hercules, M/V Midas and M/V Goldfinder, as well as Ludovico Albano, Mekonen Birhane, Edy Forlin, Christopher Gauci, Aggeliki Georgiopoulou, Manfredi Longo, Fiorenzo Pascale, Maddalena Sammartini, and Nicolas Waldmann for their assistance with data collection and processing. We are very grateful to Innomar for providing access to the SES-2000 compact Sub-Bottom Profiler. We thank the Maltese authorities for permissions to carry out the marine surveys. Tiago Alves, Davide Gamboa, Stefan Wenau and an anonymous reviewer are thanked for their constructive reviews. AM and DS are funded by the European Union's Horizon 2020 Programme (grant agreement n° 677898 (MARCAN)). This is Ismar-CNR Bologna scientific contribution n. 1985.

Appendix A. Supplementary data

Supplementary data to this article can be found online at https://doi.org/10.1016/j.marpetgeo.2019.03.033.

References

Abrams, M.A., Segall, M.P., Bartell, S.G., 2001. Best practices for detecting, identifying and characterising near-surface migration of hydrocarbons within marine sediments. In: Offshore Technology Conference, 30 April – 3 May, Houston, Texas.

Alexander, D., 1988. A review of the physical geography of Malta and its significance for tectonic geomorphology. Quat. Sci. Rev. 7, 41–43. https://doi.org/10.1016/0277-3791(88)90092-3.

Aloisi, G., Drews, M., Wallmann, K., Bohrmann, G., 2004. Fluid expulsion from the Dvurechenskii mud volcano (Black Sea). Part I. Fluid sources and relevance to Li, B, Sr, I and dissolved inorganic nitrogen cycles. Earth Planet. Sci. Lett. 225 (3–4), 347–363. https://doi.org/10.1016/j.epsl.2004.07.006.

Agius, M.R., Galea, P., 2011. A single-station automated earthquake location system at Wied Dalam Station, Malta. Seismol Res. Lett. 82 (4), 545–559.

Argnani, A., 1990. The strait of sicily rift zone: foreland deformation related to the evolution of a back-arc basin. J. Geodyn. 12 (2–4), 311–331. https://doi.org/10.1016/0264-3707(90)90028-S.

Aydin, A., 2000. Fractures, faults, and hydrocarbon entrapment, migration and flow. Mar. Petrol. Geol. 17, 797–814. https://doi.org/10.1016/S0264-8172(00)00020-9.

Ben-Avraham, Z., Grasso, M., 1991. Crustal structure variations and transcurrent faulting at the eastern and western margins of the eastern Mediterranean. Tectonophysics 196 (3–4), 269–277. https://doi.org/10.1016/0040-1951(91)90326-N.

Bense, V.F., Person, M.A., 2006. Faults as conduit-barrier systems to fluid flow in siliciclastic sedimentary aquifers. Water Resour. Res. 42 (W05421). https://doi.org/10.1029/2005WR004480.

Bezrodnykh, Y.P., Deliya, S.V., Lavrushin, V.Y., Yunin, E.A., Poshibaev, V.V., Pokrovskii, B.G., 2013. Gas seeps in the North Caspian water area. Lithol. Miner. Resour. 48 (5), 373–383. https://doi.org/10.1134/S0024490213050027.

Birhane, M., 2016. Geochemical Survey in Solution Subsidence Structures (Dolines): Examples from the Maltese Islands. University of Malta BSc. Dissertation.

Bonson, C.G., Childs, C., Walsh, J.J., Schöpfer, M.P.J., Carboni, V., 2007. Geometric and kinematic controls on the internal structure of a large normal fault in massive limestones: the Maghlaq Fault, Malta. J. Struct. Geol. 29, 336–354. https://doi.org/10.1016/j.jsg.2006.06.016.

Bosellini, A., 2002. Dinosaurs "re-write" the geodynamics of the eastern Mediterranean and the paleogeography of the Apulia Platform. Earth Sci. Rev. 59 (1–4), 211–234. https://doi.org/10.1016/S0012-8252(02)00075-2.

Boulart, C., Connelly, D.P., Mowlem, M.C., 2010. Sensors and technologies for in situ dissolved methane measurements and their evaluation using Technology Readiness Levels. Trends Anal. Chem. 29 (2), 186–195. https://doi:10.1016/j.trac.2009.12.001.

Bünz, S., Polyanov, S., Vadakkepuliyambatta, S., Consolaro, C., Mienert, J., 2012. Active gas venting through hydrate-bearing sediments on the Vestnesa Ridge, offshore W-Svalbard. Mar. Geol. 332–334, 189–197. https://doi.org/10.1016/j.margeo.2012.09.012.

Burnard, P., Bourlange, S., Henry, P., Geli, L., Tryon, M.D., Natal'in, B., Sengör, A.M.C., Özeren, M.S., Çagatay, M.N., 2012. Constraints on fluid origins and migration velocities along the Marmara Main Fault (Sea of Marmara, Turkey) using helium isotopes. Earth Planet. Sci. Lett. 341, 68–78. https://doi.org/10.1016/j.epsl.2012.05.042.

Burollet, P.F., Mugniot, J.M., Sweeney, P., 1978. The geology of the pelagian block: the margins and basins off southern Tunisia and tripolitania. In: Nairn, A.E.M., Kanes, W.H., Stehli, F.G. (Eds.), The Ocean Basins and Margins, pp. 331–359. https://doi.org/10.1007/978-1-4684-3039-4_6.

Capasso, G., Inguaggiato, S., 1998. A simple method for the determination of dissolved gases in natural waters. An application to thermal waters from Vulcano Island. Appl. Geochem. 13 (5), 631–642. https://doi.org/10.1016/S0883-2927(97)00109-1.

Caracausi, A., Favara, R., Italiano, F., Nuccio, P.M., Paonita, A., Rizzo, A., 2005. Active geodynamics of the central Mediterranean Sea: tensional tectonic evidences in western Sicily from mantle-derived helium. Geophys. Res. Lett. 32 (4), 1–5. https://doi.org/10.1029/2004GL021608.

Carminati, E., Doglioni, C., Barba, S., 2004. Reverse migration of seismicity on thrusts and normal faults. Earth Sci. Rev. 65 (3–4), 195–222. https://doi.org/10.1016/S0012-8252(03)00083-7.

Ceramicola, S., Dupré, S., Somoza, L., Woodside, J., 2018. Cold seep systems. In: Micallef, A., Krastel, S., Savini, A. (Eds.), Submarine Geomorphology. Springer, Cham, pp. 367–387. https://doi.org/https://doi.org/10.1007/978-3-319-57852-1_19.

Cicerone, R.J., Shetter, J.D., 1981. Sources of atmospheric methane: measurements in rice paddies and a discussion. J. Geophys. Res. 86 (C8), 7203–7209. https://doi.org/10.1029/JC086iC08p07203.

Civile, D., Lodolo, E., Tortorici, L., Lanzafame, G., Brancolini, G., 2008. Relationships between magmatism and tectonics in a continental rift: the Pantelleria Island region (Sicily Channel, Italy). Mar. Geol. 251 (1–2), 32–46. https://doi.org/10.1016/j.margeo.2008.01.009.

Civile, D., Lodolo, E., Accettella, D., Geletti, R., Ben-Avraham, Z., Deponte, M., Facchin, L., Ramella, R., Romeo, R., 2010. The Pantelleria graben (Sicily Channel, Central Mediterranean): an example of intraplate "passive" rift. Tectonophysics 490, 173–183. https://doi.org/10.1016/j.tecto.2010.05.008.

Coltelli, M., Cavallaro, D., D'Anna, G., D'Alessandro, A., Grassa, F., Mangano, G., Patanè, D., Gresta, S., 2016. Exploring the submarine graham bank in the sicily channel. Ann. Geophys. 59. https://doi.org/10.4401/ag-692.

Correale, A., Martelli, M., Paonita, A., Rizzo, A., Brusca, L., Scribano, V., 2012. New evidence of mantle heterogeneity beneath the Hyblean Plateau (southeast Sicily, Italy) as inferred from noble gases and geochemistry of ultramafic xenoliths. Lithos 132–133, 70–81. https://doi.org/10.1016/j.lithos.2011.11.007.

Cox, S.F., 2016. Injection-driven swarm seismicity and permeability enhancement: implications for the dynamics of hydrothermal ore systems in high fluid-flux,

overpressured faulting regimes - an invited paper. Econ. Geol. 111, 559–587. https://doi.org/10.2113/econgeo.111.3.559.
Dart, C.J., Bosence, D.W.J., McClay, K.R., 1993. Stratigraphy and structure of the Maltese graben system. J. Geol. Soc. 20, 68–86. https://doi.org/10.1144/gsjgs.150.6.1153.
Davis, A.M., 1992. Shallow gas: an overview. Cont. Shelf Res. 12 (10), 1077–1079. https://doi.org/10.1016/0278-4343(92)90069-V.
Dimmen, V., Rotevatn, A., Peacock, D.C.P., Nixon, C.W., Nærland, K., 2017. Quantifying structural controls on fluid flow: insights from carbonate-hosted fault damage zones on the Maltese Islands. J. Struct. Geol. 101, 43–57. https://doi.org/10.1016/j.jsg.2017.05.012.
Dogan, T., Mori, T., Tsunomori, F., Notsu, K., 2007. Soil H2 and CO2 surveys at several active faults in Japan. Pure Appl. Geophys. 164, 2449–2463. https://doi.org/10.1007/s00024-007-0277-5.
Espedal, H., Wahl, T., 1999. Satellite SAR oil spill detection using wind history information. Int. J. Remote Sens. 20, 49–65. https://doi.org/10.1080/014311699213596.
Etiope, G., Panieri, G., Fattorini, D., Regoli, F., Vannoli, P., Italiano, F., Locritani, M., Carmisciano, C., 2014. A thermogenic hydrocarbon seep in shallow Adriatic Sea (Italy): gas origin, sediment contamination and benthic foraminifera. Mar. Petrol. Geol. 57, 283–293. https://doi.org/10.1016/j.marpetgeo.2014.06.006.
Evans, B., Wong, T., 1992. In: Wong, B. Evans T. (Ed.), Fault Mechanics and Transport Properties of Rocks. Accademic Press Linited, New York. https://doi.org/10.1016/S0074-6142(08)62829-6.
Finetti, I., 1982. Structure, stratigraphy and evolution of central mediterranean (pelagian sea, ionian sea). Boll. Geofis. Teor. Appl. 24 (96), 247–312. https://doi.org/10.1007/s10539-010-9244-0.
Finetti, I., Del Ben, A., 2005. Crustal tectono-stratigraphic setting of the Pelagian Foreland from new CROP Seismic data. In: Finetti, I. (Ed.), CROP Project: Deep Seismic Exploration of the Central Mediterranean and Italy. Elsevier, pp. 581–595.
Finetti, I., 1984. Geophysical study of the Sicily Channel rift zone. Boll. Geofis. Teor. Appl. XXVI, 3–28.
Fisher, Q.J., Knipe, R.J., 1998. Fault sealing processes in siliciclastic sediments. Geological Society, London, Special Publications 147, 117–134. https://doi.org/10.1144/GSL.SP.1998.147.01.08.
Garven, G., Appold, M.S., Toptygina, V.I., Hazlett, T.J., 1999. Hydrogeologic modeling of the genesis of carbonate-hosted lead-zinc ores. Hydrogeol. J. 7, 108–126. https://doi.org/10.1007/s100400050183.
Gasperini, L., Polonia, A., Del Bianco, F., Etiope, G., Marinaro, G., Favali, P., Italiano, F., Çağatay, M.N., 2012. Gas seepage and seismogenic structures along the north Anatolian fault in the eastern sea of marmara. Geochem. Geophys. Geosyst. 13, 1–19. https://doi.org/10.1029/2012GC004190.
Gauci, C., 2015. Geochemical Investigations across Malta and Gozo. University of Malta BSc. Dissertation.
Gay, A., Berndt, C., 2007. Cessation/reactivation of polygonal faulting and effects on fluid flow in the Voring Basin, Norwegian Margin. J. Geol. Soc. 164, 129–141. https://doi.org/10.1144/0016-76492005-178.
Gay, A., Mourgues, R., Berndt, C., Bureau, D., Planke, S., Laurent, D., Gautier, S., Lauer, C., Loggia, D., 2012. Anatomy of a fluid pipe in the Norway Basin: initiation, propagation and 3D shape. Mar. Geol. 332 (334), 75–88. https://doi.org/10.1016/j.margeo.2012.08.010.
Géli, L., Henry, P., Zitter, T., Dupré, S., Tryon, M., Çağatay, M.N., de Lépinay, B.M., Le Pichon, X., Şengör, A.M.C., Görür, N., Natalin, B., Uçarkuş, G., Özeren, S., Volker, D., Gasperini, L., Burnard, P., Bourlange, S., the Marnaut Scientific Party, 2008. Gas emissions and active tectonics within the submerged section of the North Anatolian Fault zone in the Sea of Marmara. Earth Planet. Sci. Lett. 274, 34–39. https://doi.org/10.1016/j.epsl.2008.06.047.
Gentz, T., Damm, E., Schneider von Deimling, J., Mau, S., McGinnis, D.F., Schluter, M., 2014. A water column study of methane around gas flares located at the West Spitsbergen continental margin. Cont. Shelf Res. 72 (1), 107–118. https://doi.org/10.1016/j.csr.2013.07.013.
Goes, S., Jenny, S., Hollenstein, C., Kahle, H.G., Geiger, A., 2004. A recent tectonic reorganization in the south-central Mediterranean. Earth Planet. Sci. Lett. 226, 335–345. https://doi.org/10.1016/j.epsl.2004.07.038.
Goswami, B.K., Weitemeyer, K.A., Bünz, S., Minshull, T.A., Westbrook, G.K., Ker, S., Sinha, M.C., 2017. Variations in pockmark composition at the Vestnesa Ridge: insights from marine controlled source electromagnetic and seismic data. Geochem. Geophys. Geosyst. 18 (3), 1111–1125. https://doi.org/10.1002/2016GC006700.
Government of Malta, 1993. Geological Map of the Maltese Islands. Oil Exploration Directorate, OPM, Malta.
Gueguen, E., Doglioni, C., Fernandez, M., 1998. On the post-25 Ma geodynamic evolution of the western Mediterranean. Tectonophysics 298 (1–3), 259–269. https://doi.org/10.1016/S0040-1951(98)00189-9.
Ho, S., Hovland, M., Blouet, J.P., Wetzel, A., Imbert, P., Carruthers, D., 2018. Formation of linear planform chimneys controlled by preferential hydrocarbon leakage and anisotropic stresses in faulted fine-grained sediments, offshore Angola. Solid Earth 9, 1437–1468. https://doi.org/10.5194/se-9-1437-2018.
Holland, C.W., Etiope, G., Milkov, A.V., Michelozzi, E., Favali, P., 2003. Mud volcanoes discovered offshore Sicily. Mar. Geol. 199 (1–2), 1–6. https://doi.org/10.1016/S0025-3227(03)00125-7.
Hooper, E.C.D., 1991. Fluid migration along growth faults in compacting sediments. J. Pet. Geol. 14 (s1), 161–180. https://doi.org/10.1111/j.1747-5457.1991.tb00360.x.
Hovland, M., Gardner, J.V., Judd, A.G., 2002. The significance of pockmarks to understanding fluid flow processes and geohazards. Geofluids 2 (2), 127–136. https://doi.org/10.1046/j.1468-8123.2002.00028.x.
Illies, J.H., 1981. Graben formation — the Maltese Islands — a case history. Tectonophysics 73, 151–168. https://doi.org/10.1016/0040-1951(81)90182-7.
Italiano, F., Martelli, M., Martinelli, G., Nuccio, P.M., 2000. Geochemical evidence of melt intrusions along lithospheric faults of the Southern Apennines, Italy: geodynamic and seismogenic implications. J. Geophys. Res. 105 (B6), 13569–13578. https://doi.org/10.1029/2000JB900047.
Italiano, F., Bonfanti, P., Ditta, M., Petrini, R., Slejko, F., 2009. Helium and carbon isotopes in the dissolved gases of Friuli Region (NE Italy): geochemical evidence of CO2 production and degassing over a seismically active area. Chem. Geol. 266 (1–2), 76–85. https://doi.org/10.1016/j.chemgeo.2009.05.022.
Italiano, F., Sasmaz, A., Yuce, G., Okan, O.O., 2013. Thermal fluids along the east Anatolian fault zone (EAFZ): geochemical features and relationships with the tectonic setting. Chem. Geol. 339, 103–114. https://doi.org/10.1016/j.chemgeo.2012.07.027.
Italiano, F., De Santis, A., Favali, P., Rainone, M.L., Rusi, S., Signanini, P., 2014. The marsili volcanic Seamount (southern tyrrhenian sea): a potential offshore geothermal resource. Energies 7 (7), 4068–4086. https://doi.org/10.3390/en7074068.
Jerram, K., Weber, T.C., Beaudoin, J., 2015. Split-beam echo-sounder observations of natural methane seep variability in the northern Gulf of Mexico. Geochem. Geophys. Geosyst. 16 (3), 736–750. https://doi.org/10.1002/2014GC005429.
Jolley, S.J., Dijk, H., Lamens, J.H., Fisher, Q.J., Manzocchi, T., Eikmans, H., Huang, Y., 2007. Faulting and fault sealing in production simulation models: Brent Province, northern North Sea. Petrol. Geosci. 13, 321–340. https://doi.org/10.1144/1354-079306-733.
Jongsma, D., van Hinte, J.E., Woodside, J.M., 1985. Geologic structure and neotectonics of the north African continental margin south of sicily. Mar. Petrol. Geol. 2 (2), 156–179. https://doi.org/10.1016/0264-8172(85)90005-4.
Judd, A., Hovland, M., 2007. Seabed Fluid Flow : the Impact on Geology, Biology and the Marine Environment. Cambridge Univ. Press, Cambridge.
Judd, A.G., Hovland, M., 1992. The evidence of shallow gas in marine sediments. Cont. Shelf Res. 12 (10), 1081–1095. https://doi.org/10.1016/0278-4343(92)90070-Z.
Kennedy, B.M., Kharaka, Y.K., Evans, W.C., Ellwood, A., DePaolo, D.J., Thordsen, J., Ambats, G., Mariner, R.H., 1997. Mantle fluids in the San Andreas fault system, California. Science 278, 1278–1281. https://doi.org/10.1126/science.278.5341.1278.
King, L.H., MacLean, B., 1970. Pockmarks on the Scotian shelf. Bull. Geol. Soc. Am. 81 (10), 3142–3148. https://doi.org/10.1130/0016-7606(1970)81[3141:POTSS]2.0.CO;2.
Le Pichon, X., Engor, A.M.C., Demirba, E., Rangin, C., Imren, C., Armijo, R., Görür, N., Catay, N., Mercier de Lepinay, B., Meyer, B., Saatclar, R., Tok, B., 2001. The active main marmara fault. Earth Planet. Sci. Lett. 192, 595–616. https://doi.org/10.1016/S0012-821X(01)00449-6.
Liotta, M., Grassa, F., D'Alessandro, F., Favara, R., Gagliano Candela, E., Pisciotta, F., Scaletta, C., 2013. Isotopic composition of precipitation and groundwater in Sicily, Italy. Appl. Geochem. 34, 199–206.
MacDonald, I.R., Guinasso Jr., N.L., Ackleson, S.G., Amos, J.F., Duckworth, R., Sassen, R., Brooks, J.M., 1993. Natural oil slicks in the Gulf of Mexico visible from space. J. Geophys. Res. 98 (16), 351–364. https://doi.org/10.1029/93JC01289.
Mailloux, B.J., Person, M., Kelley, S., Dunbar, N., Cather, S., Strayer, L., Hudleston, P., 1999. Tectonic controls on the hydrogeology of the Rio Grande rift, New Mexico. Water Resour. Res. 35, 2641–2659. https://doi.org/10.1029/1999WR900110.
Maljanen, M., Komulainen, V.M., Hytonen, J., Martikainen, P.J., Laine, J., 2004. Carbon dioxide, nitrous oxide and methane dynamics in boreal organic agricultural soils with different soil characteristics. Soil Biology and Biogeochemistry 36 (11), 1801–1808. https://doi.org/10.1016/j.soilbio.2004.05.003.
Maloney, J.M., Grupe, B.M., Pasulka, A.L., Dawson, K.S., Case, D.H., Frieder, C.A., Levin, L.A., Driscoll, N.W., 2015. Transpressional segment boundaries in strike-slip fault systems offshore southern California: implications for fluid expulsion and cold seep habitats. Geophys. Res. Lett. 42, 4080–4088. https://doi.org/10.1002/2015GL063778.
Max, M.D., Kristensen, A., Michelozzi, E., 1993. Small scale Plio-Quaternary sequence stratigraphy and shallow geology of the west-central Malta Plateau. In: Max, M.D., Colantoni, P. (Eds.), Geological Development of the Sicilian-Tunisian Platform. UNESCO, Urbino, pp. 117–122.
McKenna, J.R., Blackwell, D.D., 2004. Numerical modeling of transient Basin and Range extensional geothermal systems. Geothermics 33, 457–476. https://doi.org/10.1016/j.geothermics.2003.10.001.
Meccariello, M., Ferranti, L., Barreca, G., Palano, M., 2017. New insights on the tectonics of the Lampedusa Plateau from the integration of offshore, on-land and space geodetic data. Italian Journal of Geosciences 136 (2), 206–219. https://doi.org/10.3301/IJG.2017.02.
Micallef, A., Foglini, F., Le Bas, T., Angeletti, L., Maselli, V., Pasuto, A., Taviani, M., 2013. The submerged paleolandscape of the Maltese Islands: morphology, evolution and relation to quaternary environmental change. Mar. Geol. 335, 129–147. https://doi.org/10.1016/j.margeo.2012.10.017.
Milkov, A.V., Etiope, G., 2018. Geochemistry of Shale gases from around the World. In: 80th EAGE Conference and Exhibition 2018, https://doi.org/10.3997/2214-4609.201801496.
Moore, J.C., Orange, D., Kulm, L.D., 1990. Interrelationship of fluid venting and structural evolution: Alvin observations from the frontal accretionary prism, Oregon. J. Geophys. Res. 95 (B6), 8795–8808. https://doi.org/10.1029/JB095iB06p08795.
Osler, J., Algan, O., 1999. A high resolution seismic sequence analysis of the Malta Plateau. Saclantcen Report, SR-311.
Palano, M., Ferranti, L., Monaco, C., Mattia, M., Aloisi, M., Bruno, V., Cannavò, F., Siligato, G., 2012. GPS velocity and strain fields in Sicily and southern Calabria, Italy: updated geodetic constraints on tectonic block interaction in the central Mediterranean. Rend. Online Soc. Geol. Ital. 117, B07401. https://doi.org/10.1029/2012JB009254.

Panieri, G., 2006. Foraminiferal response to an active methane seep environment: a case study from the Adriatic Sea. Marine Micropalaentology 61 (1–3), 116–130. https://doi.org/10.1016/j.marmicro.2006.05.008.

Panieri, G., Bünz, S., Fornari, D.J., Escartin, J., Serov, P., Jansson, P., Torres, M.E., Johnson, J.E., Hong, W.L., Sauer, S., Garcia, R., Gracias, N., 2017. An integrated view of the methane system in the pockmarks at Vestnesa Ridge, 79°N. Mar. Geol. 390, 282–300. https://doi.org/10.1016/j.margeo.2017.06.006.

Pedley, H.M., House, M.R., Waugh, B., 1976. The geology of Malta and Gozo. PGA (Proc. Geol. Assoc.) 87 (3), 325–341. https://doi.org/10.1016/S0016-7878(76)80005-3.

Rawling, G.C., Goodwin, L.B., Wilson, J.L., 2001. Internal architecture, permeability structure, and hydrologic significance of contrasting fault-zone types. Geology 27, 43–46. https://doi.org/10.1130/0091-7613(2001)029<0043:IAPSAH>2.0.CO.

Reuther, C.-D., Ben-Avraham, Z., Grasso, M., 1993. Origin and role of major strike-slip transfers during plate collision in the central Mediterranean. Terra. Nova 5 (3), 249–257. https://doi.org/10.1111/j.1365-3121.1993.tb00256.x.

Reuther, C.D., Eisbacher, G.H., 1985. Pantelleria Rift - crustal extension in a convergent intraplate setting. Geol. Rundsch. 74 (3), 585–597. https://doi.org/10.1007/BF01821214.

Roberts, H.H., Hardage, B. a., Shedd, W.W., Hunt, J., 2006. Seafloor reflectivity—an important seismic property for interpreting fluid/gas expulsion geology and the presence of gas hydrate. Lead. Edge 25 (5), 620. https://doi.org/10.1190/1.2202667.

Roberts, S.J., Nunn, J.A., Cathles, L., Francois-Dominique, C., 1996. Expulsion of abnormally pressured fluids along faults. J. Geophys. Res. 101 (28), 231–252. https://doi.org/10.1029/96JB02653.

Saffer, D.M., 2015. The permeability of active subduction plate boundary faults. Geofluids 15 (1–2), 193–215. https://doi.org/10.1002/9781119166573.ch18.

Saribudak, M., Hawkins, A., 2019. Hydrogeopysical characterization of the Haby crossing fault, san Antonio, Texas, USA. J. Appl. Geophys. 162, 164–173. https://doi.org/10.1016/j.jappgeo.2019.01.009.

Sauter, E.J., Muyakshin, S.I., Charlou, J.L., Schlüter, M., Boetius, A., Jerosch, K., Damm, E., Foucher, J.P., Klages, M., 2006. Methane discharge from a deep-sea submarine mud volcano into the upper water column by gas hydrate-coated methane bubbles. Earth Planet. Sci. Lett. 243, 354–365. https://doi.org/10.1016/j.epsl.2006.01.041.

Savini, A., Malinverno, E., Etiope, G., Tessarolo, C., Corselli, C., 2009. Shallow seep-related seafloor features along the Malta plateau (Sicily channel - Mediterranean Sea): morphologies and geo-environmental control of their distribution. Mar. Petrol. Geol. 26 (9), 1831–1848. https://doi.org/10.1016/j.marpetgeo.2009.04.003.

Scandone, P., 1981. Mesozoic and Cenozoic rocks from the Malta escarpment (central mediterranean). AAPG (Am. Assoc. Pet. Geol.) Bull. 65 (7), 1299–1319. https://doi.org/10.1306/03B5949F-16D1-11D7-8645000102C1865D.

Schneider von Deimling, J., Brockhoff, J., Greinert, J., 2007. Flare imaging with multibeam systems: data processing for bubble detection at seeps. Geochem. Geophys. Geosyst. 8 (6), Q06004. https://doi.org/10.1029/2007GC001577.

Spatola, D., Micallef, A., Sulli, A., Basilone, L., Ferreri, R., Basilone, G., Bonanno, A., Pulizzi, M., Mangano, S., 2018. The Graham Bank (Sicily Channel, central Mediterranean Sea): seafloor signatures of volcanic and tectonic controls. Geomorphology 318, 375–389. https://doi.org/10.1016/j.geomorph.2018.07.006.

Toki, T., Tsunogai, U., Gamo, T., Kuramoto, S., Ashi, J., 2004. Detection of low-chloride fluids beneath a cold seep field on the Nankai accretionary wedge off Kumano, south of Japan. Earth Planet. Sci. Lett. 228 (1–2), 37–47. https://doi.org/10.1016/j.epsl.2004.09.007.

Torelli, L., Grasso, M., Mazzoldi, G., Peis, D., 1998. Plio-Quaternary tectonic evolution and structure of the Catania foredeep, the northern Hyblean Plateau and the Ionian shelf (SE Sicily). Tectonophysics 298 (1–3), 209–221. https://doi.org/10.1016/S0040-1951(98)00185-1.

Vogt, P.R., Crane, K., Sundvor, E., Max, M.D., Pfirman, S.L., 1994. Methane-generated(?) pockmarks on young, thickly sedimented oceanic crust in the Arctic: Vestnesa Ridge, Fram Strait. Geology 284 (1–4), 74–85. https://doi.org/10.1130/0091-7613(1994)022<0255:MGPOYT>2.3.CO;2.

Weiss, R.F., 1974. Carbon dioxide in water and seawater: the solubility of a non-ideal gas. Mar. Chem. 13 (10), 203–215. https://doi.org/10.1016/0304-4203(74)90015-2.

Wilson, R.M., Macelloni, L., Simonetti, A., Lapham, L., Lutken, C., Sleeper, K., D'Emidio, M., Pizzi, M., Knapp, J., Chanton, J., 2014. Subsurface methane sources and migration pathways within a gas hydrate mound system, Gulf of Mexico. Geochem. Geophys. Geosyst. 15, 89–107. https://doi.org/10.1002/2013GC004888.

Winnock, E., 1981. Structure du Bloc Pelagien. In: Wezel, I.F.C. (Ed.), Sedimentary Basins of Mediterranean Margins. Tecnoprint, Bologna, pp. 445–464.

Yehya, A., Yang, Z., Rice, J.R., 2018. Effect of fault architecture and permeability evolution on response to fluid injection. J. Geophys. Res. - Solid Earth 123, 9982–9997. https://doi.org/10.1029/2018JB016550.

Zhao, C., Schaubs, P., Hobbs, B.E., 2016. Computational simulation of seepage instability problems in fluid-saturated porous rocks: potential dynamic mechanisms for controlling mineralisation patterns. Ore Geol. Rev. 79, 180–188. https://doi.org/10.1016/j.oregeorev.2016.05.002.

Zhu, L., Helmberger, D., 1996. Advancement in source estimation technique using broadband regional seismograms. Bull. Seismol. Soc. Am. 86, 1634–1641.